Green Chemistry

PAPER

View Article Online
View Journal | View Issue

Cite this: *Green Chem.*, 2025, **27**, 6260

Computational modeling-guided design of deep eutectic solvents for tailoring lignin chemistry during lignocellulose pretreatment†

Le Zhou, [a] Xianzhi Meng, [b] Weiwei Li,[a] Jiali Yu, [c] Christian O. Kemefa, [b] Susie Y. Dai,[c] Arthur J. Ragauskas [b] and Joshua S. Yuan *[a]

Lignocellulosic biorefineries offer a sustainable approach to decarbonization and biofuel production, but the full utilization of biomass components, particularly lignin, remains a challenge due to its complex structure. Deep eutectic solvents (DESs) have emerged as promising green solvents for lignin extraction and structure regulation, offering chemical tunability, recyclability, and environmental benefits. However, their potential to precisely tailor lignin linkages during biomass pretreatment has been underexplored. In this study, we integrated computational modeling with experimental validation to design DESs for lignin property regulation and efficient delignification. A total of 260 DES candidates, comprising 13 hydrogen bond acceptors (HBAs), 20 hydrogen bond donors (HBDs), and 4 lignin dimer and 4 lignin carbohydrate complex models, were screened to predict activity coefficients (γ), focusing on their effects on β-O-4 and β-5 linkages in using the Conductor-like Screening Model for Real Solvents (COSMO-RS). Nine representative DESs were synthesized and tested with hardwood pretreatment. The results showed that smaller γ values indicate stronger degradation of β-O-4 and β-5 linkages, with both the HBD and HBA playing a significant role in delignification. The β-O-4 linkage is a critical determinant of lignin's properties and applications in value-added biomaterials. Multivariate analysis reveals the overall impact of lignin structures on β-O-4 and β-5 by accounting for interactions between variables, highlighting the importance of a multivariate approach. Incorporating model compounds with etherified phenol structures and lignin–carbohydrate complexes provided a more comprehensive calculation representation of the delignification process. Experimental validation demonstrated that the 1,8-diazabicyclo[5.4.0]undec-7-ene: lactic acid DES extracted lignin with a high β-O-4 content (47%), suitable for producing carbon fibers with superior mechanical properties. In contrast, a choline chloride: lactic acid DES completely cleaved β-O-4 linkages (0%), yielding uniform lignin nanoparticles with an enhanced zeta potential. These DESs also achieved effective delignification, allowing carbohydrates to be used for biofuels. This research establishes a computational modeling-guided framework for designing DESs to achieve controllable lignin linkage profiles, optimizing both delignification efficiency and material properties. The findings provide a pathway for enhancing the economic and environmental sustainability of lignocellulosic biorefineries and expand the applications of lignin in diverse, high-value biomaterials.

Received 2nd December 2024,
Accepted 17th April 2025

DOI: 10.1039/d4gc06120a

rsc.li/greenchem

Green foundation

1 This research advances green chemistry by integrating computational modeling and experimental validation to design deep eutectic solvents (DESs) for balancing delignification and structural regulation in the lignocellulose pretreatment process. It introduces a strategy to regulate lignin linkage profiles, optimizing lignocellulosic biomass utilization for sustainable biomaterial production.

2 By screening 260 DES candidates, we identified formulations enabling tailored β-O-4 linkage content in lignin while improving lignin dissolution. High β-O-4 content lignin was utilized to produce carbon fibers with superior mechanical properties, while lignin with cleaved β-O-4 linkages yielded uniform nanoparticles, enhancing material versatility and environmental benefits. The design allowed simultaneous carbohydrate and lignin usage.

3 Expanding COSMO-RS modeling to a broader DES library and biomass types could improve precision in delignification and lignin structure tailoring. Future studies could also explore DES recyclability and scalability, maximizing economic and environmental sustainability in biorefineries.

[a]*Department of Energy, Environmental, and Chemical Engineering, Washington University in St. Louis, St Louis, MO 63130, USA. E-mail: joshua.yuan@wustl.edu*
[b]*Department of Chemical and Biomolecular Engineering, University of Tennessee Knoxville, Knoxville, TN 37996, USA*
[c]*Department of Chemical and Biomedical Engineering, University of Missouri, Columbia, MO 65211, USA*

† Electronic supplementary information (ESI) available. See DOI: https://doi.org/10.1039/d4gc06120a

Introduction

Lignocellulosic biorefineries hold promise in decarbonization and sustainable biofuel production.[1,2] Despite the potential in mitigating climate change and replacing fossil fuel usage, lignocellulosic biorefineries face substantial challenges in their commercialization, partially due to the challenge in complete utilization of biomass components including both cellulose and lignin. Lignin is a vital component of plant biomass with significant structural, ecological, and industrial importance. Its separation is crucial for various industries, particularly in the production of paper, biofuels, and bioproducts.[3–5] Advances in lignin separation techniques continue to unlock new potential for this abundant natural polymer, paving the way for more sustainable usage of both lignin and carbohydrate in biomass.[6,7] The current biorefinery design has challenges in deriving lignin with tailored structures for appropriate usage and processing into valuable products.[8] For this reason, the 'lignin first' biorefinery concept was proposed to design biorefineries to prioritize lignin usage.[9] Our previous efforts also focused on co-utilization of lignin and carbohydrate to maximize the value proposition and environmental impact of lignocellulosic biorefinery.

Deep eutectic solvents (DESs) are emerging as novel green solvents for lignocellulose pretreatment and lignin extraction owing to their outstanding characteristics of chemical and thermal stability, environmental benefits, easy preparation, and recyclability.[10–13] More importantly, DESs are composed of a combination of a hydrogen bond acceptor (HBA) and hydrogen bond donor (HBD), offering a wide variety of types with adjustable structures and properties.[14] This provides the possibility for lignin pretreatment and the regulation of the lignin linkage profile and chemical structures. Previous studies have illustrated that the glycosidic bonds in both hemicellulose and the lignin–carbohydrate complex could be cleaved during DES pretreatment.[15,16] This cleavage is crucial for breaking down the complex matrix of the biomass and freeing lignin from the hemicellulose and cellulose components.[17,18] Shen *et al.* found that the β-O-4 linkage bonds decreased from 69.52% to 11.84% after choline chloride/lactic DES pretreatment.[19] Lin *et al.* synthesized an N-heterocycle-based DES for wheat straw biomass pretreatment under different conditions and obtained lignin with controlled structural properties.[20]

Despite the previous success in DES design for delignification and biomass deconstruction, very few studies focused on tailoring the lignin structure and chemistry for downstream usage. DESs are diverse and it is not clear how DES chemistry can help tailor the lignin structure and properties, particularly, in a way to tailor the lignin linkage profile and molecular structure. For example, β-O-4 linkages are the most prevalent type of bond in lignin, accounting for the majority of its structure. Their high frequency and distribution significantly influence the overall architecture and properties of the lignin polymer.[21,22] The β-O-4 linkages in lignin are of paramount importance due to their abundance, reactivity, and potential for selective cleavage.[23] They play a critical role in the structure and functionality of lignin and are central to various industrial applications, particularly in biorefining and the production of renewable chemicals and materials.[24–26] Li *et al.* used lignin from different biomass feedstock to prepare carbon fiber and found that β-O-4 linkages are in line with the carbon fiber mechanical properties.[27] Liu *et al.* chose the organosolv pretreatment to obtain lignin with different β-O-4 linkages, the lignin with more cleaved β-O-4 linkages could be prepared the lignin nanoparticle with superior uniformity and greater stability.[28] Therefore, it is critical to control the lignin linkage profile during the DES-based lignin extraction process to achieve both delignification and the utilization of lignin for quality biomaterials. This imposes a significant challenge in DES design that has not been previously addressed: how to rapidly and effectively select the appropriate DES for lignocellulosic pretreatment and obtain the controllable linkage profile, while achieving effective delignification.

The Conductor-like Screening Model for Real Solvents (COSMO-RS) has emerged as a valuable and fast tool to predict and screen ionic liquids for biomass dissolution and DES for gas separation, and liquid–liquid extraction.[29,30] Yu *et al.* designed 19 lignin models and predicted their solubilities in 3886 ionic liquids by COSMO-RS, synthesized the 1-methyl-1-propylpyrrolidinium acetate to dissolve higher lignin in the final combined with the experimental verification.[31] Hadj-Kali *et al.* screened the activity coefficient at infinite dilution of binary azeotropic mixtures of ethanol and *n*-hexane, *n*-heptane or *n*-octane in each DES and found the tetrabutylammonium bromide/levulinic acid with a molar ratio (1 : 2) gave the best extractive performance for all systems in the experiment.[32] However, few research has focused on the prediction and design of DES simultaneously for lignin property regulation, biomass dissolution, and pretreatment efficiency.

In this study, we present a new strategy to use computational modeling to guide the DES design for both tailoring lignin properties and achieving delignification. COSMO-RS models for lignin structure were established and the model simulations were integrated with experimental verification to investigate the effects of DES on lignin dissolution and property control, specifically focusing on linkage profiles like β-O-4 linkages and β-5 bonds. We predicted and designed 260 DES, comprising 13 hydrogen bond acceptors (HBAs), 20 hydrogen bond donors (HBDs), and 8 lignin models representing minimal lignin dimers or lignin-carbohydrate complexes with β-O-4 linkages, to evaluate their activity coefficients (γ). Based on these predictions, we synthesized 9 representative DES for lignin pretreatment to validate the COSMO-RS outcomes. The screened DES were utilized to pretreat hardwood, enabling the extraction of lignin with controllable β-O-4 bond content. Lignin with a high content of β-O-4 linkages was employed to produce carbon fibers exhibiting substantially improved mechanical properties, while lignin with a lower β-O-4 content was utilized to create more uniform lignin nanoparticles. The delignification for all DES were evaluated and discussed. This research thus establishes a novel framework to design DESs for both delignification and tailoring lignin properties, allow-

ing the maximized value proposition and environmental impact for lignocellulosic biorefineries. The knowledge could also be expanded to design DESs to derive lignin with varying β-O-4 bond contents for diverse biomaterial manufacturing.

Calculation methods and details

COSOMO-RS calculation details

In this work, COSMOtherm2024 (BIOVIA) was employed for calculations, using the parameterization set to BP_TZVP_24. Hydrogen bond acceptors and donors were selected from the current databases, COSMObase2024. For molecules not included in these databases and for lignin models, Turbomole was utilized to construct and optimize the COSMO input files. The activity coefficients of the lignin models in the deep eutectic solvents (DESs) were predicted at a temperature of 393.15 K, which corresponds to the temperature used for the experimental verification.

Structures of hydrogen bond acceptors and hydrogen bond donors

As shown in Fig. 1, this research involved the combination of 13 hydrogen bond acceptors (HBAs)—including carboxylic acids, amines/amides, polyalcohols/carbohydrates, and phenolic compounds—with 20 hydrogen bond donors (HBDs), such as choline chloride, alkylammonium chlorides, alkylammonium bromides, and betaine, resulting in a total of 260 deep eutectic solvents (DES). The molar ratio was set at 1 : 2, reflecting a commonly used ratio in such formulations.

Lignin models

Lignin is biosynthesized from *p*-coumaryl, coniferyl, and sinapyl alcohols.[31] The primary monomers can form minimal dimers through β-O-4 linkages. To explore this, we constructed and optimized four dimer lignin models that contain β-O-4 linkages, as illustrated in Fig. 2a–d. These models are referred to as dimer models: the GG-lignin model, HG-lignin model, SS-lignin model, and SG-lignin model. Besides, Fig. 2e–h show lignin–carbohydrate complex (LCC) lignin models that were constructed and optimized by the esterification of glucose with phenolic hydroxyl groups; these are the glucose-GG-lignin model, glucose-HG-lignin model, glucose-SS-lignin model, and glucose-SG-lignin model.

Statistical analyses

Predicted activity coefficients (two sets of lignin models) were fitted in linear regression models to either β-O-4 content or β-5 content by Origin function 'data fitting'. The coefficients of determination (R^2) of the models were used to determine the fitting performance, with higher R^2 indicating a better fitting in the relationship between the activity coefficient (different lignin models in DESs) and β-O-4 or β-5 content. The multivariate effects among the two sets of the lignin models were analyzed using multivariate analysis of variance (MANOVA) in R. Specifically, the interactions between HG-lignin and SS-lignin models, as well as between HG-lignin and SG-lignin models, were evaluated to determine the statistical significance of their multivariate relationships. The multivariate effects of the MANOVA model were visualized with the package 'heplots'. A correlation coefficient closer to 1 indicates a strong relationship between the variables.

Experimental apparatus and procedure

Materials and reagents

Maple wood was milled and obtained from Texas A&M University, USA. Polyacrylonitrile, choline chloride, oxalic acid, lactic acid, ethylene glycol, catechol, 1,8-diazabicyclo[5.4.0] undec-7-ene, betaine, benzyltriethylammonium chloride, tetraethylammonium chloride, acetone, and *N*,*N*-dimethylformamide were purchased from Sigma-Aldrich, USA.

Deep eutectic solvent synthesis and hard wood pretreatment

Deep eutectic solvents (DESs) were synthesized by mixing hydrogen bond acceptors (HBAs) and hydrogen bond donors (HBDs) in a molar ratio of 1 : 2 at 353.15 K for 2 hours. Five HBDs—oxalic acid, lactic acid, catechol, urea, and ethylene glycol—along with five HBAs—choline chloride, betaine, 1,8-diazabicyclo[5.4.0]undec-7-ene, tetraethylammonium chloride, and benzyl triethylammonium chloride—were selected to create nine different DESs. The structures and characterization of the DES can be found in the ESI.† Dried hardwood was added to a glass tube containing the DES, with a mass ratio of corn stover to DES set at 1 : 10. The mixture was stirred at a speed of 400 rpm for 6 hours at a temperature of 393.15 K.

Lignin recovery and characterization

The details of the lignin characterization method can be found in the ESI.† An acetone aqueous solution (acetone : water = 7 : 3, volume ratio) was added and stirred for 2 hours to dissolve the lignin and DES. The mixture was then washed twice with the acetone aqueous solution and centrifuged to separate the liquids. The solid was washed and tested following the NREL standard procedure to obtain the composition. The collected liquids were rotary-evaporated at 50 °C to remove the acetone. Deionized water was added to regenerate the lignin, which was then centrifuged and washed with deionized water at least three times before being freeze-dried. Finally, the lignin regenerated from the different DES pretreatments was obtained for further characterization. Details of the lignin characterization methods can be found in the ESI.†

Preparation and characterization of lignin-based carbon fiber and lignin nanoparticles

Equal amounts of lignin regenerated from different DESs ([Ch]Cl : Lactic acid and DBU : Lactic acid) were mixed with polyacrylonitrile in *N*,*N*-dimethylformamide (solid content: 10 w%) and stirred at 25 °C for 2 hours, followed by sonication to obtain the spinning dopes. These dopes were then processed in a wet spinning unit, after which the precursor fibers under-

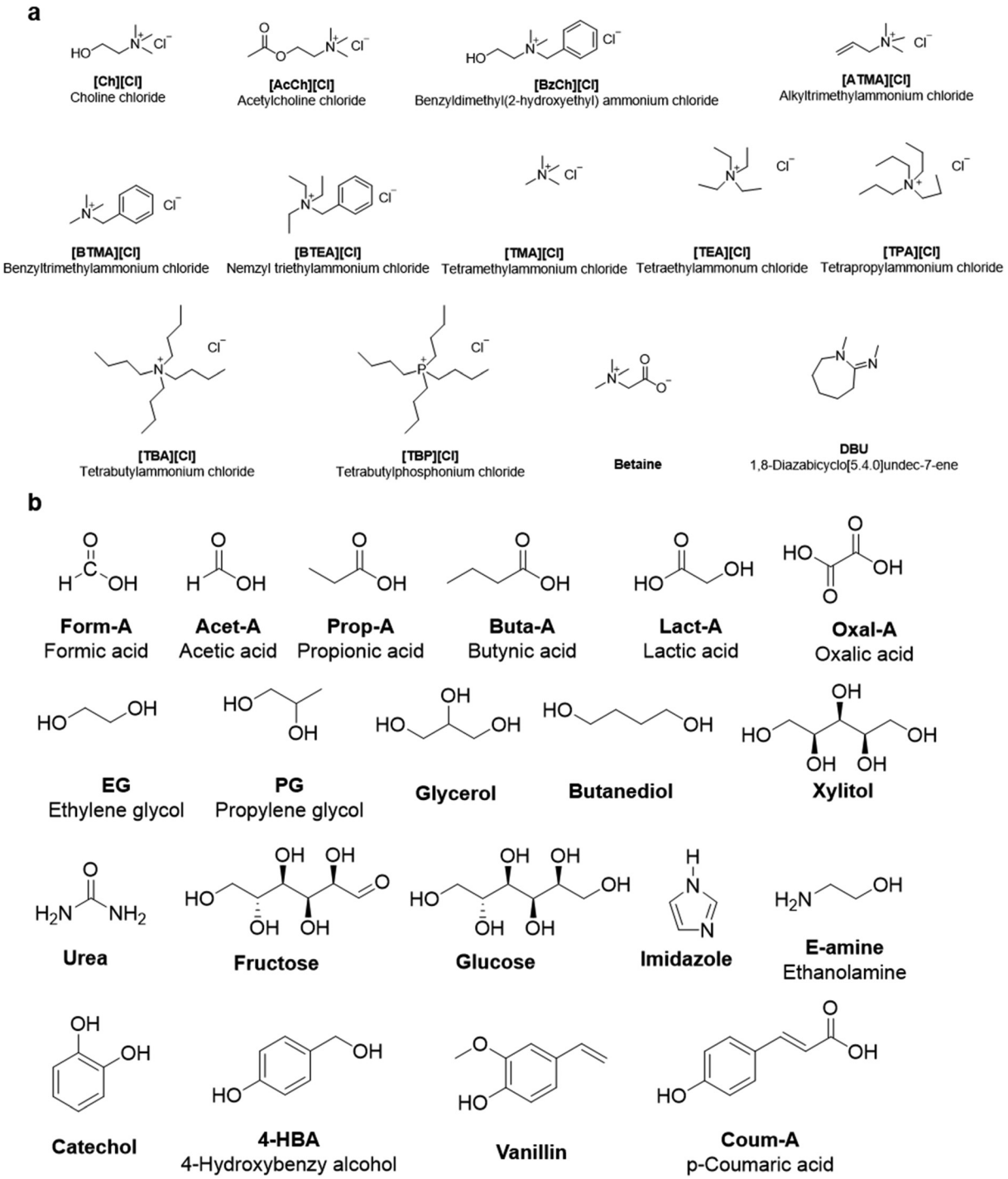

Fig. 1 Chemical structures of deep eutectic solvents. (a) Hydrogen bond acceptor and (b) hydrogen bond donor.

went thermal stabilization and carbonization to form lignin-based carbon fibers, as described in our previous work.[27,33] The diameter and morphology of the fibers were observed using Scanning Electron Microscopy (SEM). The mechanical properties of the carbon fibers, including tensile strength, elongation, and modulus of elongation, were measured using a TestResources universal mechanical tester.

Lignin nanoparticles (LNP) were fabricated *via* dialysis based on our previous research.[28,34] Lignin regenerated from different DESs was dissolved in acetone at a concentration of 10 mg mL^{-1} and then loaded into a dialysis bag. This bag was placed in deionized water with stirring. The deionized water was repeatedly replaced to remove the acetone, leading to the formation of lignin nanoparticles. The particle size and zeta

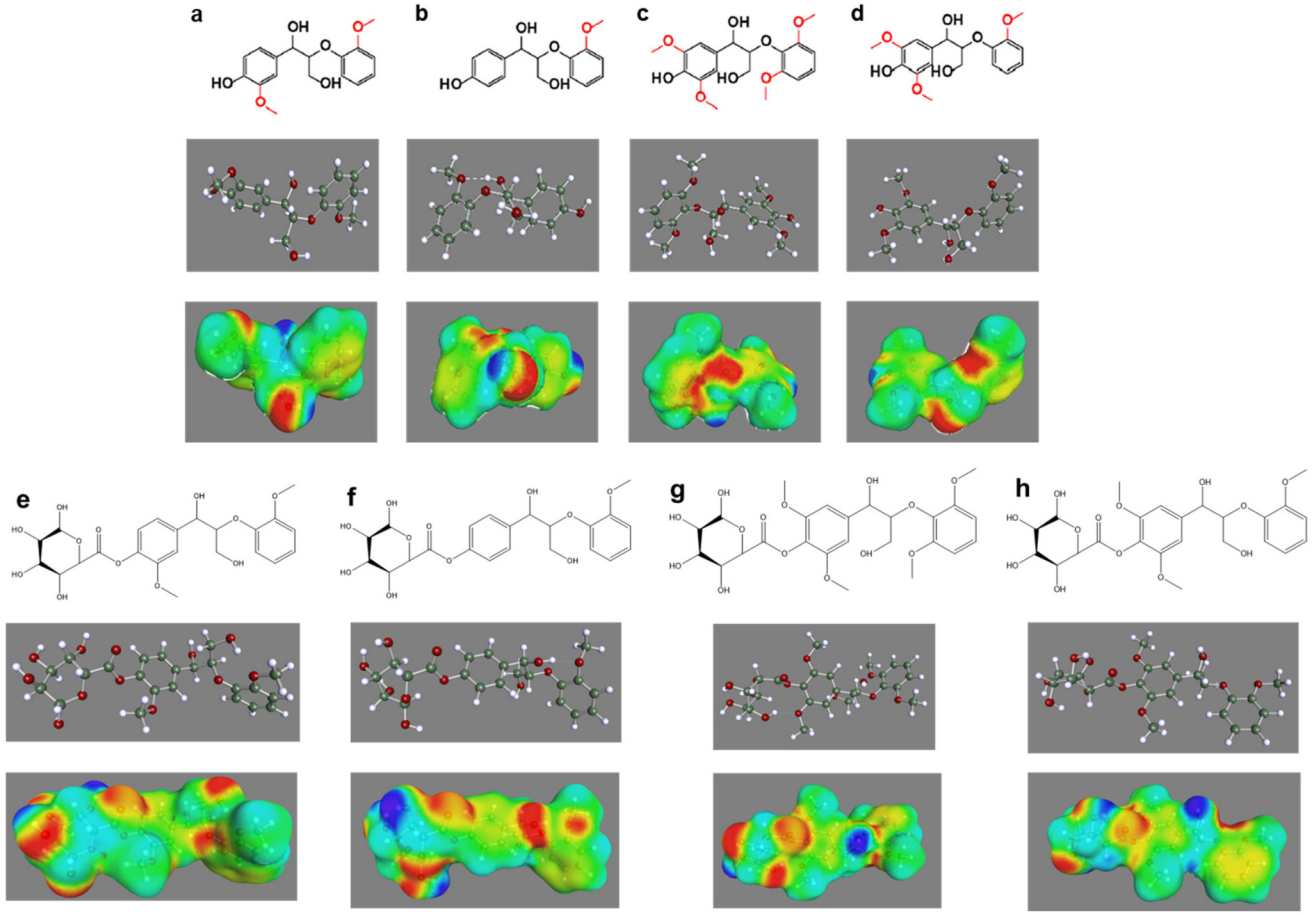

Fig. 2 Optimized structures and charge surface regions of eight lignin models. (a) GG-lignin model; (b) HG-lignin model; (c) SS-lignin; (d) SG-lignin model; (e) glucose-GG-lignin model; (f) glucose-HG-lignin model; (g) glucose-SS-lignin; and (h) glucose-SG-lignin model.

potential of the LNP dispersion were measured using Dynamic Light Scattering (Malvern ZEN 3600 Zetasizer). The morphology of LNP was characterized by scanning electron microscopy (Thermo Fisher Quattro S ESEM).

Results and discussion

Computational modeling for DES design to improve delignification and tailor lignin chemistry

In order to control the lignin structure during delignification, we first established a lignin structure model in COSMO-RS for studying the interaction with the DES. Unlike the previous lignin model, which only used the H/S/G monomer structure, we selected four dimer lignin structures containing β-O-4 bonds. This laid the foundation for the regulation of the β-O-4 linkage during the calculation of the delignification process. In COSMO-RS, the σ potential and σ profiles are typically used to analyze the affinity between the system and the polar σ surface.[35] As shown in Fig. S5,† there are three main regions in the σ potential: the hydrogen bond donor region ($\sigma < -0.0082$ e Å^{-2}), the nonpolar region (-0.0082 e Å$^{-2} < \sigma < +0.0082$ e Å^{-2}), and the hydrogen bond acceptor region ($+0.0082$ e Å$^{-2} < \sigma$). Fig. S5† shows that the different lignin models have similar σ potentials. For SG-lignin and SS-lignin, their higher hydrogen bond acceptor values in the sigma profile indicate their stronger capacities to form hydrogen bonds, corresponding to stronger disruption of the lignin structure. These interactions play a crucial role in the dissolution of lignin in DES systems by facilitating the disruption of key linkages within the lignin structure, such as β-O-4 bonds. In Fig. S5,† the sigma profiles of all four lignin models are largely consistent, with each exhibiting higher values in the hydrogen bond acceptor regions. This consistency further supports that the DES provides the necessary molecular environment to engage with and destabilize these critical linkages in lignin, regardless of their structural model variations.

Even though COSMO-RS was employed as an effective tool to quickly predict and design ionic liquids for the dissolution of cellulose and lignin, few research studies predicted and designed DESs for biomass dissolution and pretreatment while controlling the lignin structure. In order to achieve this unprecedented goal, the logarithmic activity coefficients of lignin in the DES were calculated. The DES pretreatment of

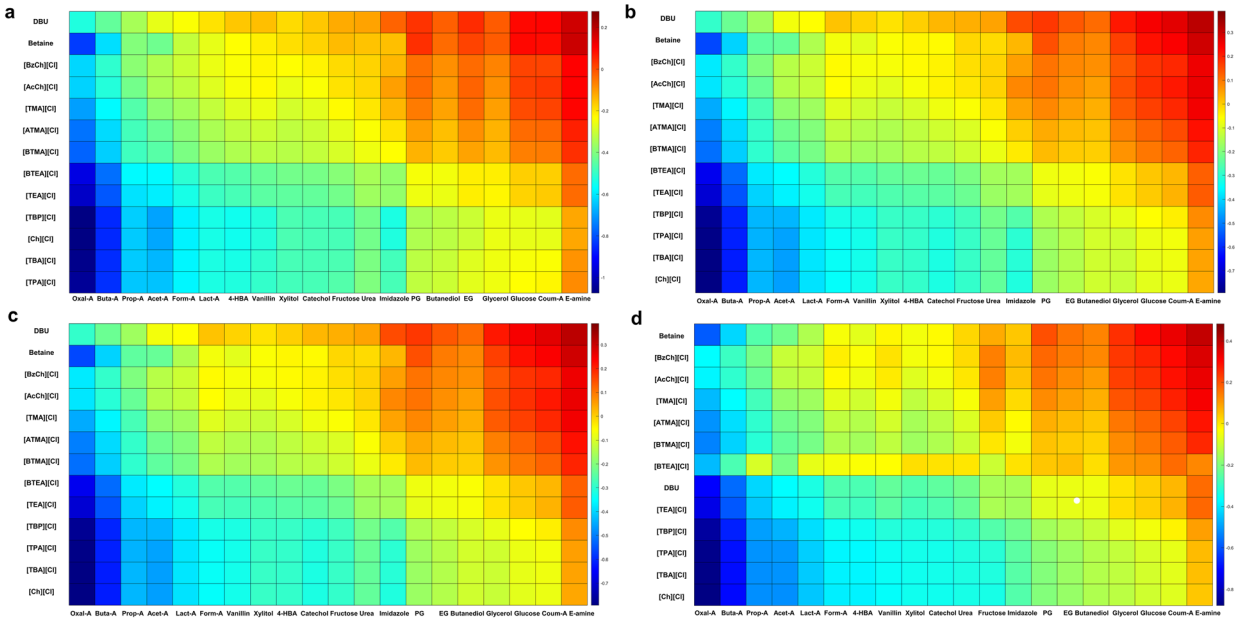

Fig. 3 The logarithmic activity coefficient (ln γ) prediction of the lignin model in 260 DESs at 393.15 K. (a) HG-lignin model; (b) SS-lignin model; (c) GG-lignin model; and (d) SG-lignin model.

corn stover targets the regulation and disruption of β-O-4 linkages. By breaking these bonds, DESs facilitate lignin depolymerization and dissolution while enhancing cellulose accessibility.[13,36] As shown in Fig. 3a, the logarithmic activity coefficients of the HG-lignin model in 260 DESs, composed of 13 HBAs and 20 HBDs, were analyzed. A bluer color indicates a more negative activity coefficient, signifying a stronger dissolving capability of the DES for lignin. This stronger dissolving capability correlates with an enhanced ability to break β-O-4 linkages, the primary structural bonds in lignin, driving its depolymerization and enabling precise structural regulation.[37] Furthermore, it can be inferred that HBDs play a primary role, while HBAs act mainly in synergy in the process of lignin dissolution by the DES, particularly in breaking β-O-4 linkages, similar to the behavior observed in ionic liquid dissolution of lignin.[38–41] Oxalic acid, butanoic acid, propionic acid, and carboxy acid, as HBDs in DESs, exhibit a high lignin solubility. As for the HBAs, tetrapropylammonium chloride, tetrabutylammonium chloride, and choline chloride, these DESs could break more β-O-4 bonds to dissolve more lignin. Fig. 3b–d illustrate the impact on different lignin models, showing the activity coefficients of the SS-lignin, GG-lignin, and SG-lignin models in DESs. Although the activity coefficients vary numerically among the four lignin models, their trends across different types of DESs are largely consistent. This consistency arises because all four lignin models share the same phenolic ring structure, differing only in the alkyl side chains on the phenolic rings.[42] This finding suggests that any of the lignin models with β-O-4 linkages can be used to represent lignin for modeling the structural regulation and dissolution processes of lignin. More importantly, it highlights which combinations of HBAs and HBDs have great potential in β-O-4 bond disruption of lignocellulose for lignin dissolution. This enables the design of novel DESs for balancing delignification and structural regulation in the lignocellulose pretreatment process.

Experimental validation verifies that the computational models can effectively guide the design of DESs for lignin dissolution and delignification

In order to verify the model outcome, nine representative DESs were selected for experimental synthesis and lignin dissolution at a temperature of 393.15 K to validate the predictions made by COSMO-RS. For the selection of HBAs, it primarily focused on choline-based compounds, alkyl ammonium salts, and heterobicyclic compounds, as they exhibit better solubility for lignin based on COSMO-RS prediction. For the selection of HBDs, it mainly used carboxylic acids, amines, polyols, and phenolic compounds, which represent a wide range of functional groups that interact differently with lignin. To investigate the effects of HBDs and HBAs on lignin dissolution and structure, five HBDs with strong β-O-4 bond disruption and high lignin dissolution—oxalic acid, lactic acid, catechol, urea, and ethylene glycol—were chosen, along with five HBAs—choline chloride, betaine, 1,8-diazabicyclo[5.4.0]undec-7-ene, tetraethylammonium chloride, and benzyl triethylammonium chloride—to create nine different DESs. These substances were selected based on their molecular structures, hydrogen bonding capacity, and compatibility with lignin, as predicted by COSMO calculations.

As shown in Table S1,† when choline chloride is used as the HBA and oxalic acid and lactic acid as the HBDs, the delignification rates of wood after pretreatment are relatively high, reaching 80.6% and 71.3%, respectively. This is consistent with the results from our previous model calculations,

where the activity coefficients of the lignin model in these DESs are more negative, allowing for the disruption of more β-O-4 bonds, thus dissolving and extracting more lignin. However, focusing solely on the delignification rate is not enough. When customizing lignin for downstream applications, the structure of the lignin is far more important.

The computational models can effectively guide DES design for tailoring lignin structures during dissolution

The lignin structure analysis indicated that DESs designed by the computational modeling effectively tailored the lignin linkage profile. FT-IR spectra of regenerated lignin are shown in Fig. S6,† displaying absorption bands characteristic of the G, H, and S units of lignin. For example, the peak at 1266 cm^{-1} is attributed to derivatives of the G unit, while the band at 836 cm^{-1} corresponds to aromatic C–H out-of-plane deformation in G and S units. Additionally, the hydroxyl groups in the lignin regenerated from the nine DESs were quantified using ^{31}P NMR, as shown in Fig. S6.† The results indicate that the hydroxyl content of lignin extracted using the nine different DES pretreatments does not vary significantly, remaining at approximately 5 mmol g^{-1}. As shown in Fig. S7,† 2D HSQC NMR was utilized to investigate how different DES treatments affect the structure of lignin extracted from wood, specifically measuring the content of β-O-4 and β-5 bonds. As shown in Table 1, a more negative activity coefficient corresponds to greater destructiveness to lignin during the pretreatment of corn stalks, resulting in lower β-O-4 bond content. The four lignin models exhibited the most positive activity coefficients in the DES (DBU-lactic acid), leading to the highest experimentally measured β-O-4 bond content, which reached up to 47%. In contrast, the DES formulations (ChCl-lactic acid and ChCl-oxalic acid) had more negative activity coefficients, resulting in greater destruction of lignin; in these cases, NMR could no longer detect β-O-4 bonds. The β-5 bond measurements showed similar trends to those of the β-O-4 bond: the more negative the activity coefficient, the lower the β-5 bond content in the lignin. An analysis of the effect of HBA on lignin destructiveness can be observed from the β-O-4 and β-5 bond content of ChCl-lactic acid, BTEACl-lactic acid, and TEACl-lactic acid. The β-O-4 and β-5 bond contents of lignin were relatively similar, aligning with the predicted results. With the same HBA, however, the β-O-4 and β-5 bond contents of lignin varied significantly depending on the HBD composition in the DES (ChCl-catechol, ChCl-urea, ChCl-lactic acid, ChCl-oxalic acid). This indicates that DESs with quaternary ammonium salts (*e.g.*, ChCl) as HBAs generally follow the pattern of HBD playing the primary role and HBA serving as a secondary factor for breaking the lignin linkages. Nevertheless, this trend does not necessarily hold for DESs with structurally distinct HBAs, such as heterobicyclic compounds. For instance, the comparison between ChCl/lactic acid (0% β-O-4 content) and DBU/lactic acid (47% β-O-4 content) demonstrates that the HBA significantly influences the degradation of lignin linkages, particularly when heterobicyclic HBAs are involved. Therefore, the roles of HBAs and HBDs are not universally fixed but are context-dependent, with both components being important when structurally diverse HBAs are used.

To determine whether the two sets of lignin models (four dimer lignin models and four lignin–carbohydrate complex lignin models) can accurately represent lignin for COSMO-RS calculations, a simple linear regression analysis was conducted on the β-O-4 and β-5 bond content in relation to the activity coefficients of the two sets of lignin models in DESs. As shown in Fig. 4a, the R^2 values for predicting β-O-4 bond content using the HG-lignin, SS-lignin, GG-lignin, and SG-lignin models were 0.3531, 0.2507, 0.4408, and 0.2139, respectively. The lower R^2 values compared to other biomass dissolution predictions can be attributed to the complexity of the lignin β-O-4 bond. In contrast, the predictions for β-5 bond content, presented in Fig. 4b, yielded higher R^2 values of 0.7215, 0.6547, 0.7360, and 0.6291 for the HG-lignin, SS-lignin, GG-lignin, and SG-lignin models, respectively, indicating better predictive performance than for β-O-4 bond content. These findings suggest that the GG-lignin model is the optimal choice for describing lignin dimers, as it exhibits the highest R^2 values for both β-O-4 and β-5 bond contents. However, the cleavage of lignin–carbohydrate complexes is a key factor in the delignification of lignocellulosic biomass. As shown in Fig. 4d and e, a simple linear regression of LCC models was performed and the improvement in the linear regression coefficients was minimal, and the fit for the β-O-5 linkage was worse compared to that of the dimer lignin models.

Table 1 The β-O-4 and β-5 bond content of lignin and activity coefficients in 9 DESs (dimer lignin models)

			ln *r*			
DES	β-O-4 (%)	β-5 (%)	HG-lignin	SS-lignin	GG-lignin	SG-lignin
[Ch][Cl]-ethylene glycol	29	6	−0.26053	−0.1095	−0.3213	−0.133
[Ch][Cl]-catechol	28	2.4	−0.47671	−0.2896	−0.5517	−0.3333
[Ch][Cl]-urea	26	0	−0.53292	−0.3081	−0.7137	−0.3287
[Ch][Cl]-lactic acid	0	3.4	−0.55135	−0.3437	−0.6698	−0.3887
[Ch][Cl]-oxalic acid	0	0	−0.85569	−0.6139	−0.9743	−0.6967
DBU-lactic acid	47	11.1	−0.09878	−0.0471	−0.135	−0.0463
Betaine-lactic acid	15	11.6	−0.16178	0.0152	−0.3198	0.0516
[BTEA][Cl]-lactic acid	2.4	2.9	−0.33917	−0.1472	−0.4889	−0.1356
[TEA][Cl]-lactic acid	2.2	1	−0.45824	−0.2565	−0.5948	−0.2629

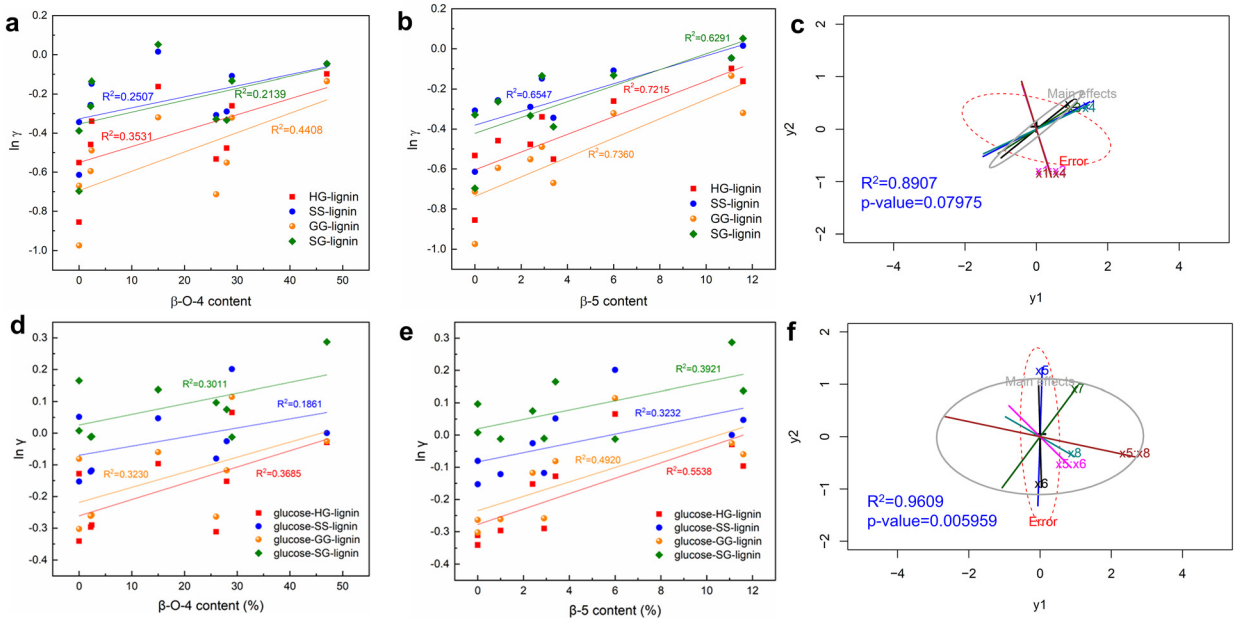

Fig. 4 Lignin carbon–carbon bond content and fitting results of computational predictions. (a) Experimental β-O-4 of lignin in 9 DESs plotted against ln γ (dimer lignin model); (b) β-5 bond content of lignin in 9 DESs plotted against ln γ (dimer lignin model); (c) the fitting curves from multivariate analysis of the impact of the four dimer lignin models on β-O-4 and β-5 bond content (*y*1-β-O-4 bond content, *y*2-β-5 bond content, *x*1-HG-lignin, *x*2-SS-lignin, *x*3-GG-lignin, *x*4-SG-lignin model); (d) experimental β-O-4 of lignin in 9 DESs plotted against ln γ (LCC lignin model); (e) β-5 bond content of lignin in 9 DESs plotted against ln γ (LCC lignin model); (f) the fitting curves multivariate analysis of the impact of the four LCC lignin models on β-O-4 and β-5 bond content (*y*1-β-O-4 bond content, *y*2-β-5 bond content, *x*5-glucose-HG-lignin, *x*6-glucose-SS-lignin, *x*7-glucose-GG-lignin, *x*8-glucose-SG-lignin model).

We address the limitation of linear regression by improving our statistical modeling with multi-variate analysis to take into consideration multiple linkages and structural factors. The actual composition of lignin is highly complex, and the DES delignification process is of multivariate nature. For example, the deconstruction of β-O-4 bonds may impact the deconstruction of β-5 bonds. The factors have interactions with one another. For this reason, a simple linear regression of each linkage with the DES activity co-efficiencies cannot capture these multivariate processes. Therefore, MANOVA was introduced to further investigate the influence of the two sets of lignin models on the prediction of multiple linkages and structural factors.

As shown in Fig. 4c, HG-lignin is more influential than the other lignin models when considering both β-O-4 and β-5 bond contents simultaneously, with the SS-lignin and SG-lignin models also contributing to some extent. Each lignin model significantly affects β-O-4 bond content, which has a larger scale compared to β-5 bond content. When the lines extend beyond the error area, they indicate a meaningful effect. When analyzing two lignin models together, the lines ($x1 + x2$) and ($x1 + x4$) fall outside the error and main effect areas, suggesting that for the β-O-4 bond in lignocellulosic biomass, the HG-β-O-4 lignin model plays a dominant role, followed by the SS-β-O-4 and SG-β-O-4 lignin models, while the GG-β-O-4 lignin model has a negligible impact. For the LCC models, as shown in Fig. 4f, glucose-SG-lignin and glucose-SS-lignin models are more influential than the other two LCC models because the lines (*x*7 and *x*8) fall outside the error areas and the lines (*x*5 and *x*6) are within the error and main effect areas. It is worth noting that for the LCC models, the R^2 value is 0.9609 with a *p*-value of 0.005959, whereas for the dimer lignin models, the R^2 value is 0.8907 with a *p*-value of 0.07975.

The results highlighted several aspects. First, as compared to regular lignin dimer models, the LCC models provided a more comprehensive representation of the real lignin structure, and thus dropped the *p*-value from the marginally significant range (0.07975) to the highly significant range (0.005959). Second, from the methodology perspective, MANOVA is more reliable than simple linear regression and yielded higher R^2 for correlation between activity coefficients and lignin structures. MANOVA takes into account the interactions between dependent variables, providing a more comprehensive assessment of the overall impact of the lignin structures. In contrast, linear regression analyzes β-O-4 and β-5 separately, potentially missing important multivariate effects. The significant MANOVA result suggests that the lignin model structures have an overall effect on the dissolution of β-O-4 and β-5 by the DES. Even though the individual linear regressions do not show significant effects, the multivariate analysis yielded more significant correlation between DES activity co-efficiencies and lignin linkages. The multivariate effects indicated that the lignin structure needs to be considered as a whole when

studying the impact by the DES and its correlation with activity coefficient, instead of individual linkages. Furthermore, it appears that incorporating model compounds with both etherified phenol structures and lignin–carbohydrate complexes would provide a more comprehensive representation of the delignification process than modeling lignin alone. Third, the analysis highlights that COSMO-RS can effectively identify the DES with a low activity coefficient to deconstruct lignin structures. The method substantially improves the efficiency of DES design and allows us to tailor the DES to preferably deconstruct certain structures to tailor the chemical structures of the extracted lignin. Even though linear regressions of each linkage (β-O-4 or β-5) with a DES activity coefficient did not reach statistical significance, they did yield decent R values, indicating that there is selectivity in linkage deconstruction by the designed DES. We thus used this knowledge and approach to guide us in designing more efficient DESs for lignin structure tuning.

DES-tailored lignin structure empowered quality biomaterial design

Based on the COSMO-RS calculations and experimental validation, we found that the DES (DBU-LA) pretreatment results in lignin with a higher β-O-4 linkage content (47%), while the DES (ChCl-LA) pretreatment yields lignin with a lower β-O-4 linkage content (0%). Consequently, these two types of lignin were selected for investigating the effects of different DES treatments on lignin for carbon fiber production. As shown in Fig. 5a–e, the carbon fibers derived from these two types of lignin exhibit similar uniform geometrical morphologies in the fiber axis directions. However, Fig. 5g, h and S8† show that the carbon fibers prepared from DBU-LA extracted lignin have a smaller diameter and more uniform distribution, with an average diameter of 6.17 μm, compared to 7.49 μm for the carbon fibers prepared from ChCl-LA extracted lignin. This may be attributed to the better compatibility and interaction between DBU extracted lignin and polyacrylonitrile, resulting in better spinnability. The DBU-LA-extracted lignin has a higher content of β-O-4 linkages. Our previous studies have revealed that the linkage profile plays an important role in lignin-PAN miscibility and the resulting carbon fiber crystallinity and performance.[24,27,43] The smaller diameter also contributes to the enhanced mechanical properties in subsequent stages. In addition, Fig. 5c and f reveal that the carbon fibers prepared from DBU-LA extracted lignin have a compact structure at the cross-section, while the carbon fibers prepared from ChCl-LA extracted lignin contain some voids. This difference again may be attributed to the higher content of β-O-4 linkages in the DBU extracted -lignin. The improved miscibility and compatibility with polyacrylonitrile could have contributed towards improving the spinnability and thermal process.[44] The cleavage of β-O-4 linkages occurs during the extraction of lignin in the DES. However, these linkages are crucial for lignin-based biomaterials, as their content is significantly cor-

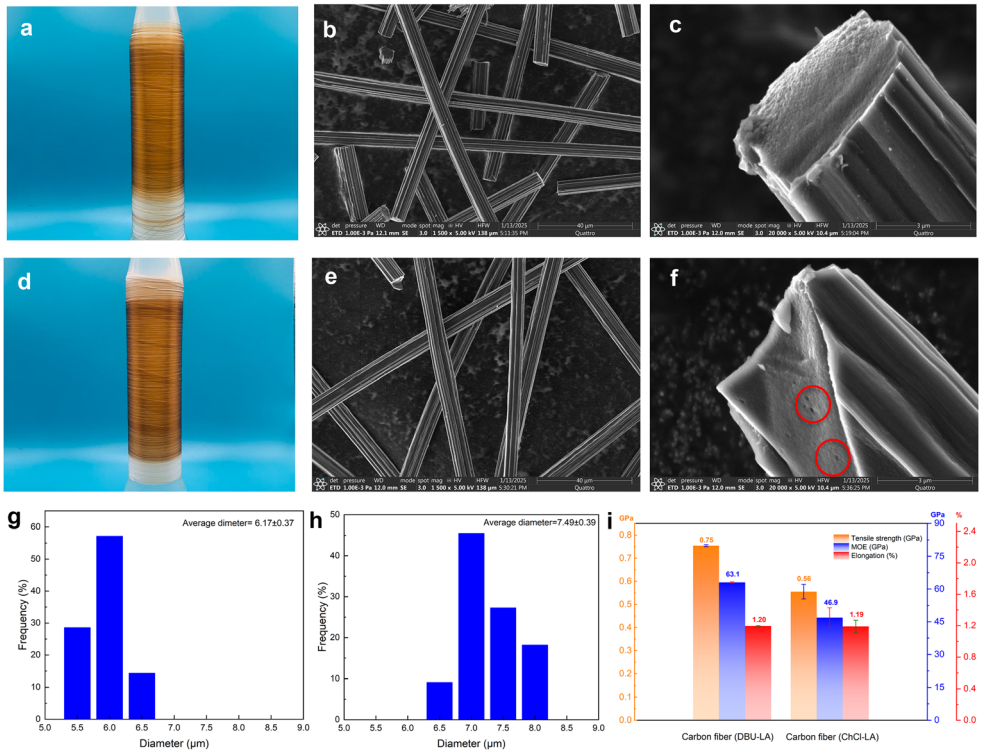

Fig. 5 Morphology and mechanical properties of lignin-based carbon fiber. (a, b and c) Photograph and SEM image of DBU-LA pretreated lignin carbon fiber; (d, e and f) photograph and SEM image of ChCl-LA pretreated lignin carbon fiber; (g and h) dimeter of the DBU-LA pretreated lignin and ChCl-LA pretreated lignin carbon fiber; (i) mechanical performance of lignin-based carbon fiber.

related with the tensile strength and elastic modulus of lignin carbon fibers, according to our previous study.[27,45] The mechanical performance of these two lignin-based carbon fibers is presented in Fig. 5e. Lignin regenerated from DES (DBU-LA), which has a higher β-O-4 content (47%), exhibits a tensile strength of up to 1.02 GPa, nearly twice the strength of the carbon fiber derived from ChCl-LA pretreated lignin, which has a tensile strength of only 0.52 GPa and a β-O-4 content of 0%. Additionally, the elongation at break for DBU-LA pretreated lignin carbon fiber is greater than that of ChCl-LA pretreated lignin carbon fiber, measuring 1.69% compared to 0.93%, respectively. The modulus of elasticity (MOE) of the carbon fibers also varies among different DES-pretreated lignin. Notably, the MOE of DBU-LA pretreated lignin carbon fiber is 61.31 GPa, which is higher than that of the ChCl-LA pretreated lignin carbon fiber, which measures 55.59 GPa. These results indicate that DBU-LA pretreated lignin carbon fibers possess superior mechanical properties compared to those from ChCl-LA pretreatment. Furthermore, carbon fibers produced from lignin with a high β-O-4 content exhibit enhanced mechanical properties. Thus, varying DES pretreatments of hardwood can effectively regulate the β-O-4 content in lignin, resulting in carbon fibers with distinct mechanical characteristics.

Lignin with a higher cleavage of β-O-4 linkages can yield lignin nanoparticles (LNPs) with superior uniformity and greater stability. For LNP preparation, ChCl-LA pretreated lignin and DBU-LA pretreated lignin were selected as representatives of low (0%) and high (47%) β-O-4 contents, respectively. The performance of the LNPs is illustrated in Table 2 and Fig. S9.† The average diameter of LNPs prepared from ChCl-LA pretreated lignin is 211 nm, significantly smaller than the average diameter of LNPs derived from DBU-LA pretreated lignin, which is 349 nm. Notably, as shown in Fig. S9,† LNPs from DBU-LA pretreated lignin tend to further aggregate into micron-sized particles, which negatively impacts the uniformity of the LNPs. The zeta potential measurements further demonstrate that LNPs prepared from ChCl-LA pretreated lignin exhibit superior stability. As indicated in Table 2, the zeta potentials of the LNP dispersions prepared from ChCl-LA and DBU-LA pretreated lignin are 25.2 mV and 5.6 mV, respectively; a higher zeta potential value correlates with greater stability of the LNPs. These results suggest that LNPs prepared from lignin with low β-O-4 content possess enhanced properties.[28] These LNPs can be used further in controlled nutrient release fertilizers, enhancing efficiency and sustainability, while in electrochemistry, they function as eco-friendly materials for energy storage applications such as batteries and supercapacitors.[46,47] DESs can effectively regulate and achieve low β-O-4 content in lignin during the pretreatment of corn stover, resulting in the production of LNPs with smaller diameters and superior uniformity.

Table 2 The particle size and zeta potential of lignin nanoparticles

LNP	*Z*-Average (nm)	PDI	Zeta potential (mV)	Conductivity (mS cm^{-1})
ChCl-LA	211.3	0.112	25.2	0.678
DBU-LA	349.2	0.268	5.5	0.142

Conclusion

In this study, we combine computational model calculations with experimental verification to investigate the effects of deep eutectic solvents on lignocellulose pretreatment efficiency and lignin properties simultaneously. In particular, we focused on delignification and tuning the linkage profile. Our goal is to predict and design DESs for balancing delignification and structural regulation in the lignocellulose pretreatment process, while simultaneously achieving regulation of the β-O-4 bond content in lignin. We evaluated 260 DESs, consisting of 13 hydrogen bond acceptors (HBAs) and 20 hydrogen bond donors (HBDs), and modeled four minimal lignin dimers with β-O-4 linkages and four lignin–carbohydrate complex lignin models to predict their activity coefficients (γ). Based on the γ predictions, we synthesized nine representative DESs for lignin pretreatment and characterization. The results indicate that a smaller γ corresponds to a stronger destructive effect on β-O-4 and β-5 linkages, with HBDs playing a major role in the dissolution and extraction of lignin, while HBAs may exert synergistic effects due to their minimal impact on γ. Multivariate analysis of the calculated γ and experimental β-O-4 and β-5 bond contents revealed that the HG-lignin model predominantly contributes to the β-O-4 bonds in wood lignocellulosic biomass, followed by the SS-lignin and SG-lignin models, with the GG-lignin model being nearly negligible. It is worth noting that for the LCC models, the R^2 value is 0.9609 with a *p*-value of 0.005959, whereas for the dimer lignin models, the R^2 value is 0.8907 with a *p*-value of 0.07975. What's more, incorporating model compounds with etherified phenol structures and lignin–carbohydrate complexes would provide a more comprehensive representation of the delignification process. MANOVA reveals the overall impact of lignin structures on β-O-4 and β-5 by accounting for interactions between variables, highlighting the importance of a multivariate approach. This method can be used to guide future DES design for various purposes. Based on computational modeling, we identified two prescreened DESs—choline chloride: lactic acid and 1,8-diazabicyclo[5.4.0]undec-7-ene: lactic acid—which resulted in lignin with higher (47%) and lower (0%) β-O-4 linkage contents, respectively. These two DESs were selected for the pretreatment of hardwood to obtain lignin suitable for the preparation of carbon fibers and lignin nanoparticles. Lignin regenerated from ChCl-lactic acid exhibited low β-O-4 content (0%), resulting in lignin nanoparticles with smaller sizes and a higher zeta potential under the same conditions. In contrast, lignin regenerated from DBU-lactic acid, which had a higher β-O-4 content (47%), produced carbon fibers with superior mechanical performance. This work establishes a novel paradigm for modeling DESs for delignification

and lignin property control. In particular, we have designed DESs with the ability to tailor the β-O-4 linkages of lignin using computational model calculations, empowering the manufacturing of quality materials. The study thus opens new avenues on computational modeling-guided design of DES to maximize the value proposition and environmental impact of biomass utilization.

Data availability

The authors confirm that the data supporting the findings of this study are available within the article and its ESI.†

Conflicts of interest

There are no conflicts to declare.

Acknowledgements

We would like to acknowledge financial support received from the Lucy & Stanley Lopata Professorship and U.S. Department of Energy Projects DE EE 0008250 and DE EE 0009763.

References

1 B. Long, F. Zhang, S. Y. Dai, M. Foston, Y. J. Tang and J. S. Yuan, *Nat. Rev. Bioeng.*, 2024, **3**, 230–244.
2 D. J. Peterson, C. Paek, L. Tao, R. Davis, X. W. Chen, R. Brunecky, M. Fowler and R. Elander, *Biotechnol. Biofuels Bioprod.*, 2024, **17**(52), 1–21.
3 J. S. Yuan, M. J. Pavlovich, A. J. Ragauskas and B. X. Han, *Trends Biotechnol.*, 2022, **40**, 1395–1398.
4 A. J. Ragauskas, G. T. Beckham, M. J. Biddy, R. Chandra, F. Chen, M. F. Davis, B. H. Davison, R. A. Dixon, P. Gilna, M. Keller, P. Langan, A. K. Naskar, J. N. Saddler, T. J. Tschaplinski, G. A. Tuskan and C. E. Wyman, *Science*, 2014, **344**, 1246843.
5 S. X. Xie, S. Sun, F. R. Lin, M. Z. Li, Y. Q. Pu, Y. B. Cheng, B. Xu, Z. H. Liu, L. D. Sousa, B. E. Dale, A. J. Ragauskas, S. Y. Dai and J. S. Yuan, *Adv. Sci.*, 2019, **6**, 1801980.
6 Z. H. Liu, N. J. Hao, Y. Y. Wang, C. Dou, F. R. Lin, R. C. Shen, R. Bura, D. B. Hodge, B. E. Dale, A. J. Ragauskas, B. Yang and J. S. Yuan, *Nat. Commun.*, 2021, **12**, 3912.
7 Y. D. Li, R. Davis, E. C. D. Tan, J. Dempsey, K. Lynch, D. A. Sievers and X. W. Chen, *ACS Sustainable Chem. Eng.*, 2023, **11**, 15876–15886.
8 J. Li, C. Hu, J. Arreola-Vargas, K. Chen and J. S. Yuan, *Trends Biotechnol.*, 2022, **40**, 1535–1549.
9 B. C. Klein, B. Scheidemantle, R. J. Hanes, A. W. Bartling, N. J. Grundl, R. J. Clark, M. J. Biddy, L. Tao, C. T. Trinh, A. M. Guss, C. E. Wyman, A. J. Ragauskas, E. G. Webb, B. H. Davison and C. M. Cai, *Energy Environ. Sci.*, 2024, **17**, 1202–1215.
10 J. Y. Cheng, C. Huang, Y. N. Zhan, X. Z. Liu, J. Wang, X. Z. Meng, C. G. Yoo, G. G. Fang and A. J. Ragauskas, *Green Chem.*, 2023, **25**, 1571–1581.
11 R. G. Zou, X. Zhou, M. Qian, C. X. Wang, D. Boldor, H. W. Lei and X. Zhang, *Green Chem.*, 2024, **26**, 1153–1169.
12 X. C. Shi, Z. B. Wang, S. Y. Liu, Q. Q. Xia, Y. Z. Liu, W. S. Chen, H. P. Yu and K. Zhang, *Nat. Sustainability*, 2024, 7(3), 315–325.
13 D. J. Cronin, X. W. Chen, L. Moghaddam and X. Zhang, *ChemSusChem*, 2020, **13**, 4678–4690.
14 D. K. Yu, D. P. Jiang, Z. M. Xue and T. C. Mu, *Green Chem.*, 2024, **26**, 7478–7507.
15 J. Y. Cheng, X. Z. Liu, C. Huang, Y. N. Zhan, C. X. Huang, T. J. Chen, X. Z. Meng, C. G. Yoo, G. G. Fang and A. J. Ragauskas, *Green Chem.*, 2023, **25**, 6270–6281.
16 H. C. Li, X. Li, D. Q. Li, J. K. Zhang, H. Nawaz, T. T. You and F. Xu, *Bioresour. Technol.*, 2022, **351**, 126993.
17 S. Hong, X. J. Shen, T. Q. Yuan, H. P. Yu and F. Wang, *Trends Chem.*, 2023, **5**, 827–839.
18 Q. L. Liu, X. H. Zhao, D. K. Yu, H. T. Yu, Y. B. Zhang, Z. M. Xue and T. C. Mu, *Green Chem.*, 2019, **21**, 5291–5297.
19 X. J. Shen, J. L. Wen, Q. Q. Mei, X. Chen, D. Sun, T. Q. Yuan and R. C. Sun, *Green Chem.*, 2019, **21**, 275–283.
20 K. T. Lin, C. X. Wang, M. F. Guo, E. Apra, R. S. Ma, A. J. Ragauskas and X. Zhang, *Proc. Natl. Acad. Sci. U. S. A.*, 2023, **120**, e2307323120.
21 Y. Y. Yu, W. K. Cheng, Y. L. Li, T. Wang, Q. Q. Xia, Y. Z. Liu and H. P. Yu, *Green Chem.*, 2022, **24**, 3257–3268.
22 L. Ramos, G. Maltempi-Mendes, A. F. Siqueira, D. A. D. Napoleao and A. K. Chandel, *React. Chem. Eng.*, 2024, **10**, 119–129.
23 Q. Q. Xia, Y. Z. Liu, J. Meng, W. K. Cheng, W. S. Chen, S. X. Liu, Y. X. Liu, J. Li and H. P. Yu, *Green Chem.*, 2018, **20**, 2711–2721.
24 J. H. Li, C. Hu, Y. Y. Wang, X. Meng, S. S. Xiang, C. Bakker, K. Plaza, J. A. Ragauskas, Y. S. Dai and S. J. Yuan, *Matter*, 2022, **5**, 3513–3529.
25 J. H. Li, X. H. Li, Y. B. Da, J. L. Yu, B. Long, P. Zhang, C. Bakker, B. A. McCarl, J. S. Yuan and S. Y. Dai, *Nat. Commun.*, 2022, **13**, 4368.
26 T. S. Lankiewicz, H. Choudhary, Y. Gao, B. Amer, S. P. Lillington, P. A. Leggieri, J. L. Brown, C. L. Swift, A. Lipzen, H. Y. S. Na, M. Amirebrahimi, M. K. Theodorou, E. E. K. Baidoo, K. Barry, I. V. Grigoriev, V. I. Timokhin, J. Gladden, S. Singh, J. C. Mortimer, J. Ralph, B. A. Simmons, S. W. Singer and M. A. O'Malley, *Nat. Microbiol.*, 2023, **8**, 596–610.
27 Q. Li, C. Hu, M. J. Li, P. Truong, J. H. Li, H. S. Lin, M. T. Naik, S. S. Xiang, B. E. Jackson, W. Kuo, W. H. Wu, Y. Q. Pu, A. J. Ragauskas and J. S. Yuan, *Green Chem.*, 2021, **23**, 3725–3739.
28 Z. H. Liu, N. J. Hao, S. Shinde, M. L. Olson, S. Bhagia, J. R. Dunlap, K. C. Kao, X. F. Kang, A. J. Ragauskas and J. S. Yuan, *ACS Sustainable Chem. Eng.*, 2019, **7**, 2634–2647.

29 M. Ayuso, S. Mateo, A. Belinchon, P. Navarro, J. Palomar, J. Garcia and F. Rodriguez, *J. Mol. Liq.*, 2023, **380**, 121710.
30 Y. S. Zhao, R. Gani, R. M. Afzal, X. P. Zhang and S. J. Zhang, *AIChE J.*, 2017, **63**, 1353–1367.
31 K. Yu, W. L. Ding, Y. M. Lu, Y. L. Wang, Y. R. Liu, G. Y. Liu, F. Huo and H. Y. He, *J. Mol. Liq.*, 2022, **348**, 118007.
32 M. K. Hadj-Kali, H. F. Hizaddin, I. Wazeer, L. El Blidi, S. Mulyono and M. A. Hashim, *Fluid Phase Equilib.*, 2017, **448**, 105–115.
33 C. Hu, M. Z. Zhao, Q. Li, Z. H. Liu, N. J. Hao, X. Z. Meng, J. H. Li, F. R. Lin, C. X. Li, L. Fang, S. Y. Dai, A. J. Ragauskas, H. J. Sue and J. S. Yuan, *ChemSusChem*, 2021, **14**, 4260–4269.
34 Z. H. Liu, N. J. Hao, S. Shinde, Y. Q. Pu, X. F. Kang, A. J. Ragauskas and J. S. Yuan, *Green Chem.*, 2019, **21**, 245–260.
35 L. Chen, X. Liu, Y. K. Sun, L. Zhou, Y. Nie and K. D. Song, *ACS Sustainable Chem. Eng.*, 2020, **8**, 18314–18323.
36 X. L. Zhou, X. Z. Liu, Y. N. Zhan, H. Y. Bian, S. F. Wu, H. Q. Dai, F. M. Liang, X. Z. Meng, C. Huang, G. G. Fang and A. J. Ragauskas, *Chem. Eng. J.*, 2024, **487**, 150407.
37 Y. X. Wang, J. E. Ryu, K. H. Kim, X. Z. Meng, Y. Q. Pu, Y. Tian, A. Eudes, G. Leem, A. J. Ragauskas and C. G. Yoo, *AIChE J.*, 2023, **69**, e18227.
38 Y. H. Chu and X. Z. He, *ACS Omega*, 2019, **4**, 2337–2343.
39 M. Mohan, B. A. Simmons, K. L. Sale and S. Singh, *Sci. Rep.*, 2023, **13**, 271.
40 L. Zhou, Y. X. Liu, J. T. Zhang, Q. G. Li, M. L. Yuan and Z. Q. Kang, *J. Mol. Liq.*, 2024, **407**, 125214.
41 L. Zhou, X. X. Li, Z. Q. Kang, X. Liu, Q. G. Li, L. Y. Ma, H. S. Gao and Y. Nie, *ACS Appl. Polym. Mater.*, 2022, **4**, 6649–6658.
42 M. Mohan, K. X. Huang, V. R. Pidatala, B. A. Simmons, S. Singh, K. L. Sale and J. M. Gladden, *Green Chem.*, 2022, **24**, 1165–1176.
43 Q. Li, S. X. Xie, W. K. Serem, M. T. Naik, L. Liu and J. S. Yuan, *Green Chem.*, 2017, **19**, 1628–1634.
44 Q. Li, W. K. Serem, W. Dai, Y. Yue, M. T. Naik, S. X. Xie, P. Karki, L. Liu, H. J. Sue, H. Liang, F. J. Zhou and J. S. Yuan, *J. Mater. Chem. A*, 2017, **5**, 12740–12746.
45 Q. Li, M. J. Li, H. S. Lin, C. Hu, P. Truong, T. Zhang, H. J. Sue, Y. Q. Pu, A. J. Ragauskas and J. S. Yuan, *ChemSusChem*, 2019, **12**, 3249–3256.
46 Y. T. Wang, X. N. Yu, S. S. Ma, S. L. Cao, X. F. Yuan, W. B. Zhu and H. L. Wang, *Green Chem.*, 2024, **26**, 42–56.
47 W. J. Chen, C. X. Zhao, B. Q. Li, T. Q. Yuan and Q. Zhang, *Green Chem.*, 2022, **24**, 565–584.